PREPARATION AND CHARACTERIZATION

OF EVAPORATED CDS FILMS

by

THEODORE M. VANDERWEL, B.Eng

PART B: McMASTER (OFF CAMPUS) PROJECT*

A Report Submitted to the School of Graduate Studies

in Partial Fulfilment of the Requirements

for the Degree

Master of Engineering

Department of Engineering Physics

McMaster University

Hamilton, Ontario, Canada

April 1978

*One of two project reports: The other part is designated
                           PART A: ON-CAMPUS PROJECT.

MASTER OF ENGINEERING (1978)　　　　　　　　McMASTER UNIVERSITY
(Department of Engineering Physics)　　　　　Hamilton, Ontario


TITLE:　　　　　　PREPARATION AND CHARACTERIZATION OF
　　　　　　　　　EVAPORATED CdS FILMS

AUTHOR:　　　　　THEODORE M. VANDERWEL, B.ENG, McMaster University


SUPERVISOR:　　　Dr. R.A. Clarke


NUMBER OF PAGES:　iv, 44

# ABSTRACT

As part of a $CdS-Cu_2S$ thin film solar cell research project, a CdS evaporation system was designed and built using an Edwards 19E6 coating unit. With the overall aims of the project in mind, the apparatus was designed as part of a $CdS-Cu_2S$ dual, in situ, evaporation system. CdS films, ranging in thickness from $1\mu$ to $25\mu$, produced by this system, were characterized optically, electrically and crystallographically as functions of the various evaporation parameters.

## ACKNOWLEDGEMENTS

## INDEX

# SECTION 1

## INTRODUCTION

### 1.1 Introduction

The work reported here is a small part of a Solar Program being carried out by Garrett Manufacturing Limited of Rexdale, Ontario. The remainder of this section is intended to define the scope of the work and show how it fits into the overall program. Section 2 describes the design and construction of the evaporation apparatus used, while Section 3 presents and discusses the experimental results obtained on the films produced by this equipment.

### 1.2 Background

Todays energy outlook is rapidly approaching a critical situation. The decreasing availability and increasing costs of fossil fuels, coupled with present public opinion trends against the radioactivity hazards of nuclear generating systems, have made solar energy an attractive and almost economically viable alternative.

For the past year Garrett Manufacturing, in conjunction with McMaster University, has undertaken studies of various processes for the fabrication of thin film $Cu_2S/CdS$ solar cells[1]

with the long term aim of establishing an industrial production system for the manufacture of a reliable and efficient solar power source.

The structure of the $Cu_2S/CdS$ thin film cell is shown in Figure 1.2.1. Several preparation methods were considered by Garrett for the $Cu_2S$ layer, including sulphurization of an evaporated Cu film or evaporation of a $Cu_2S$ pressbar, but the CdS films were all prepared by vacuum deposition from a resistively heated CdS source powder.

## 1.3  Project Aims

This report covers the evaporation system, including a proposed in vacuo deposition of both the CdS and $Cu_2S$ layers, and the preparation of 1μ to 20μ thick CdS films using the system. The films were characterized in several ways and these characteristics were correlated with the evaporation conditions. In particular, the effects of substrate temperature, source temperature, film deposition rate, and film thickness were studied. Film evaluation was done optically, using a Beckman Spectrophotometer, crystallographically, using x-ray diffraction, and electrically, using an automated Hall Effect System.

Figure 1.2.1: Typical Cu$_2$S-CdS Solar Cell Structure.

1$\mu$ EVAPORATED AU CONTACT

.08$\mu$ Cu$_2$S

20$\mu$ EVAPORATED CdS

1$\mu$ Zn PLATED

50$\mu$ Cu FOIL
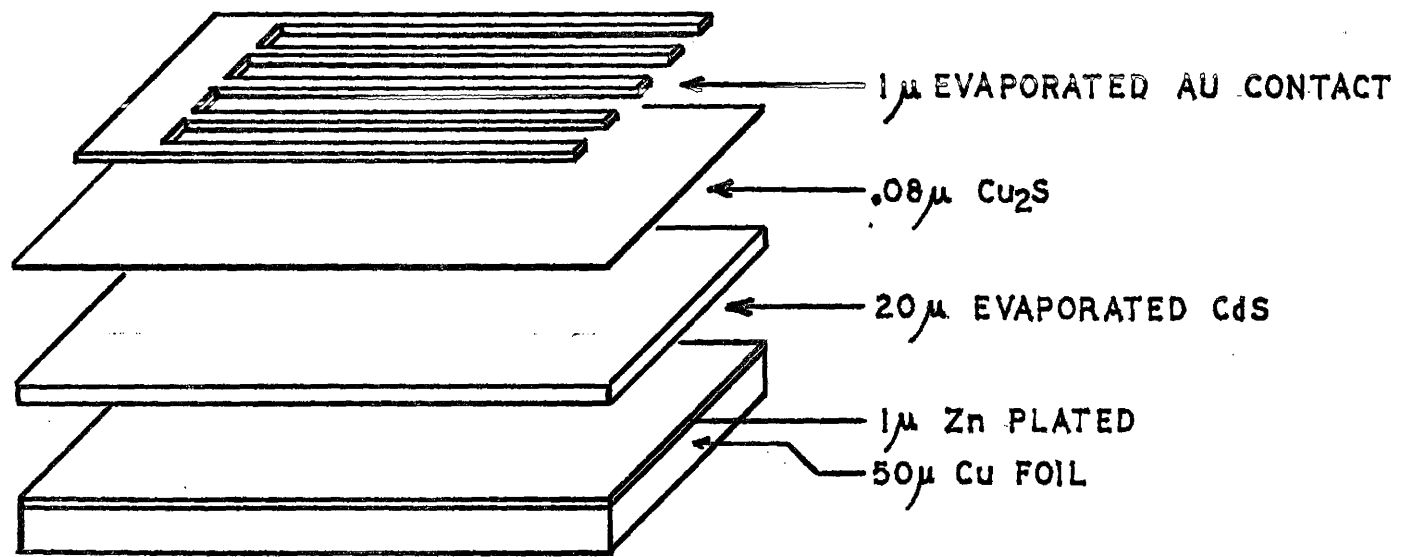
NOT DRAWN TO SCALE

# SECTION 2

## APPARATUS

### 2.1 Introduction

CdS films were prepared by vacuum deposition using an Edwards 19E6 coating unit capable of a pressure of $5 \times 10^{-7}$ torr. A 1 to 2 c.c. charge of electronic grade CdS is heated in a capped carbon crucible by a cylindrical tantalum filament to a temperature of 800° to 1200°C and the CdS vapour stream exits through a hole in the crucible cap. A quartz wool plug is used to prevent spattering. To recharge the source, the crucible is raised by means of the stainless steel support.

The substrate (Zn plated Cu foil), several test samples and monitoring probes are held 10 to 15 cm above the source in a temperature controlled frame. Shuttering is accomplished by removing the substrate holder assembly from the evaporant stream. The 1μ thick Zn plating of the Cu foil was done at Garrett using a zinc fluoroborate electroplating process. For more details see the Garrett project reports[1] or A.K. Graham's "Electroplating Engineering Handbook" (Reinhold Pub. Corp. 1971).

Temperature measurements were made using Chromel-Alumel thermocouples in the source and substrate assemblies. To avoid spurious thermoelectric effects, the chromel and alumel wires were fed intact out of the vacuum chamber and copper wire extensions were attached well away from any variable temperature areas (Figure 2.1.1).

4

vacuum chamber

O-ring

silver solder

glass & metal
feedthrough

KN
KP } T/C wire
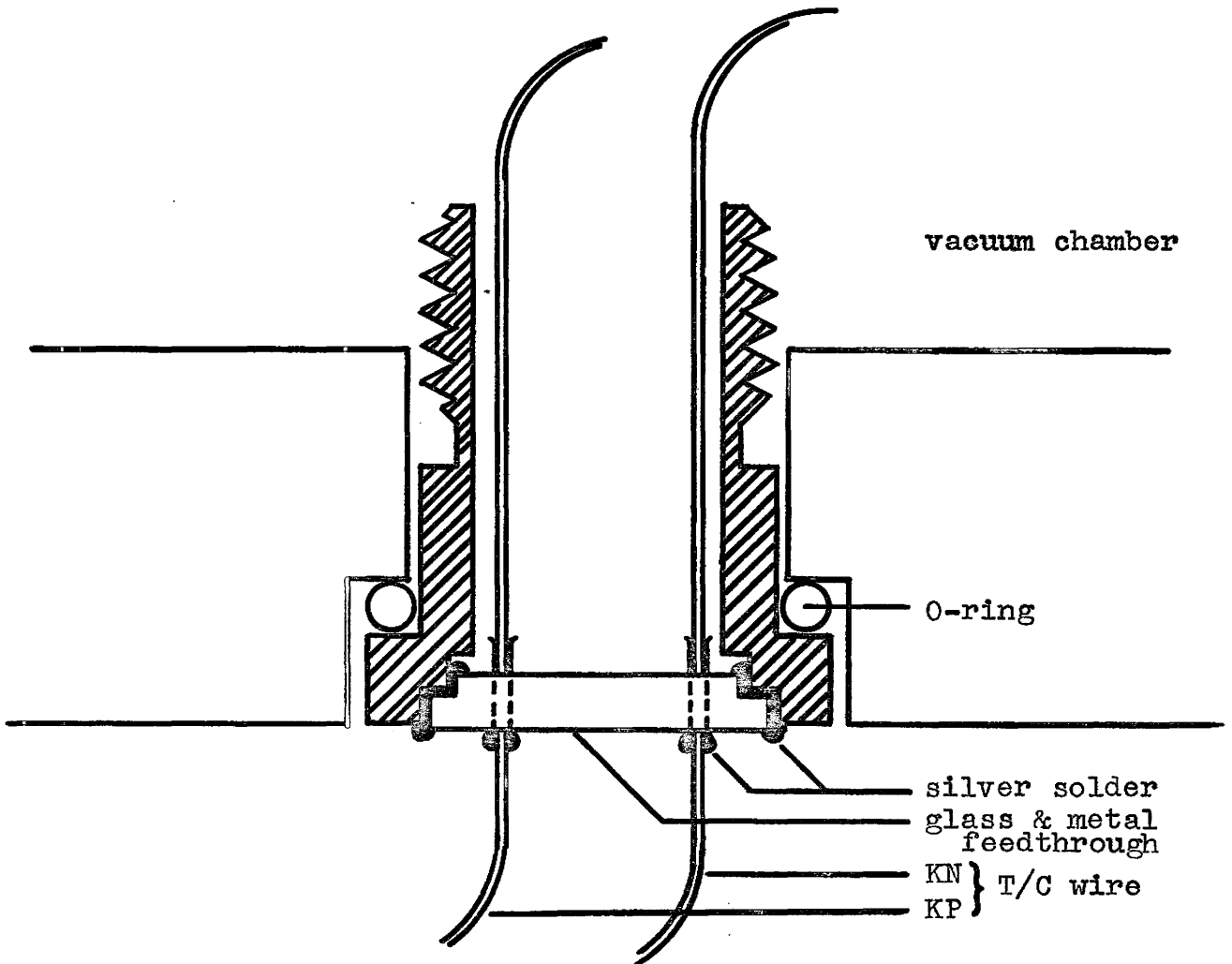
Figure 2.1.1: Thermocouple feedthrough

## 2.2  Source Details

In a preliminary examination of the CdS evaporation process, a small alumina crucible of about 0.75 c.c. capacity, heated by a coiled tungsten wire, was used as the source.  Although the CdS did not wet the alumina, this arrangement presented several problems. The small size was the main difficulty.  As a quartz wool plug was necessary to prevent spattering, the CdS charge that could be used was too small for the thick (20μ) films required for the hetero-junction cells they were to be prepared for.  Also, thermometry was difficult, and a good thermal contact between the thermocouple junction and the alumina source was never achieved, giving a much lower source temperature reading than was actually the case.

Another problem was the broad evaporant stream due to the wide mouth of the alumina crucible.  This made evaporant containment very difficult, resulting in layers of CdS on the bell jar interior as well as the possibility of sulphur contamination of the diffusion pump oil.

The above considerations led to the carbon crucible and tantalum filament arrangement shown in Figures 2.2.1 and 2.2.2. This crucible design includes an increased charge volume for CdS and quartz wool, good thermal tracking by the thermocouple in the base of the crucible, and a narrower evaporant stream due to the 0.25" diameter hole in the crucible cap.  The crucible was machined in the Ultra Purified Grade Graphite, UF-4S, available from Ultra Products, Bay City, Michigan, and it was found that the CdS did not

graphite crucible cap

graphite crucible

T/C junction

graphite table
stainless steel tubing
  crucible support
copper electrode

.01" Ta foil

.002" tantalum foil
  filament
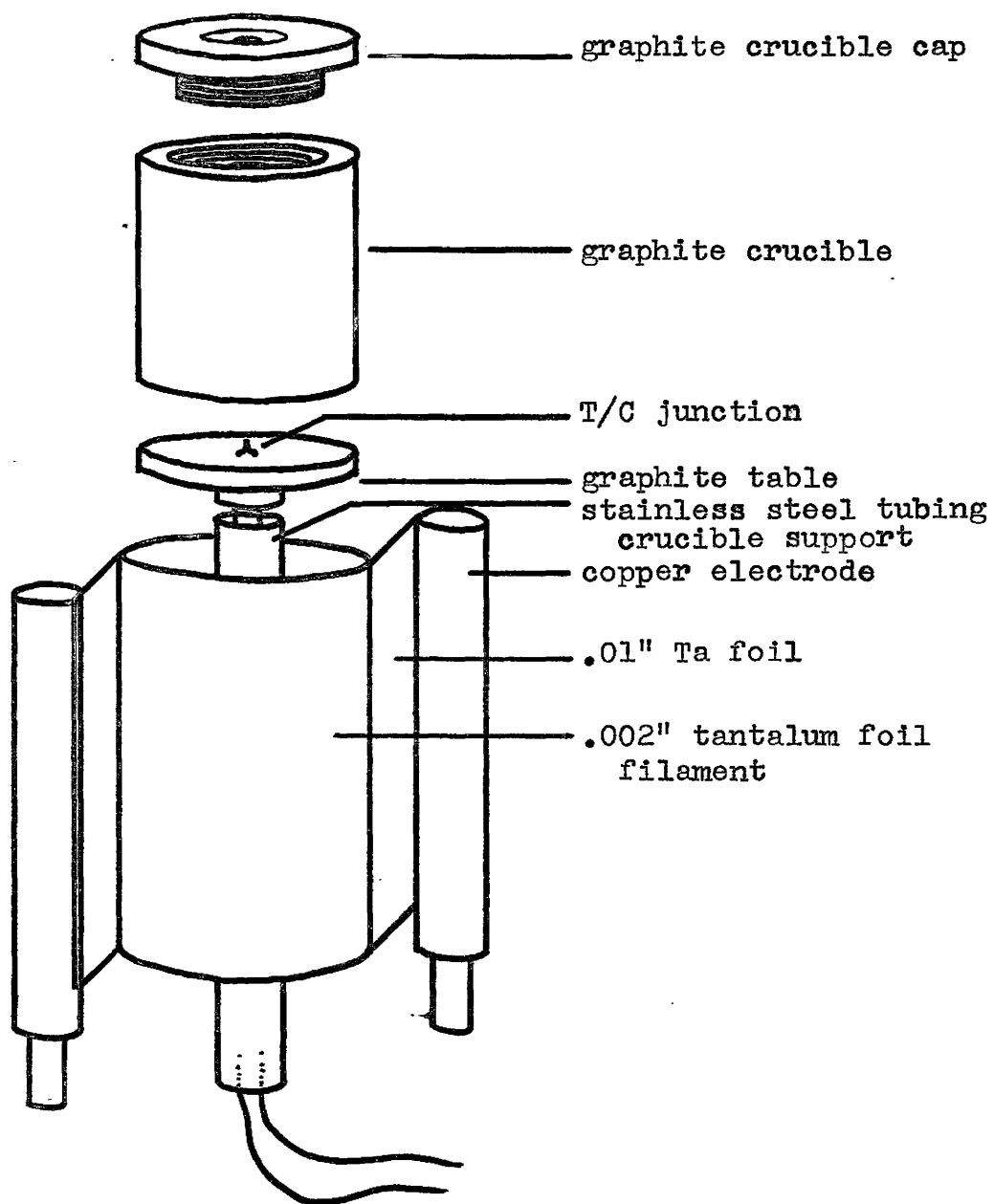
Figure 2.2.1: Carbon crucible and Tantalum filament

TOP VIEWS      ELEVATION      SCALE:  |__1 INCH__|
(CROSS-SECTION)
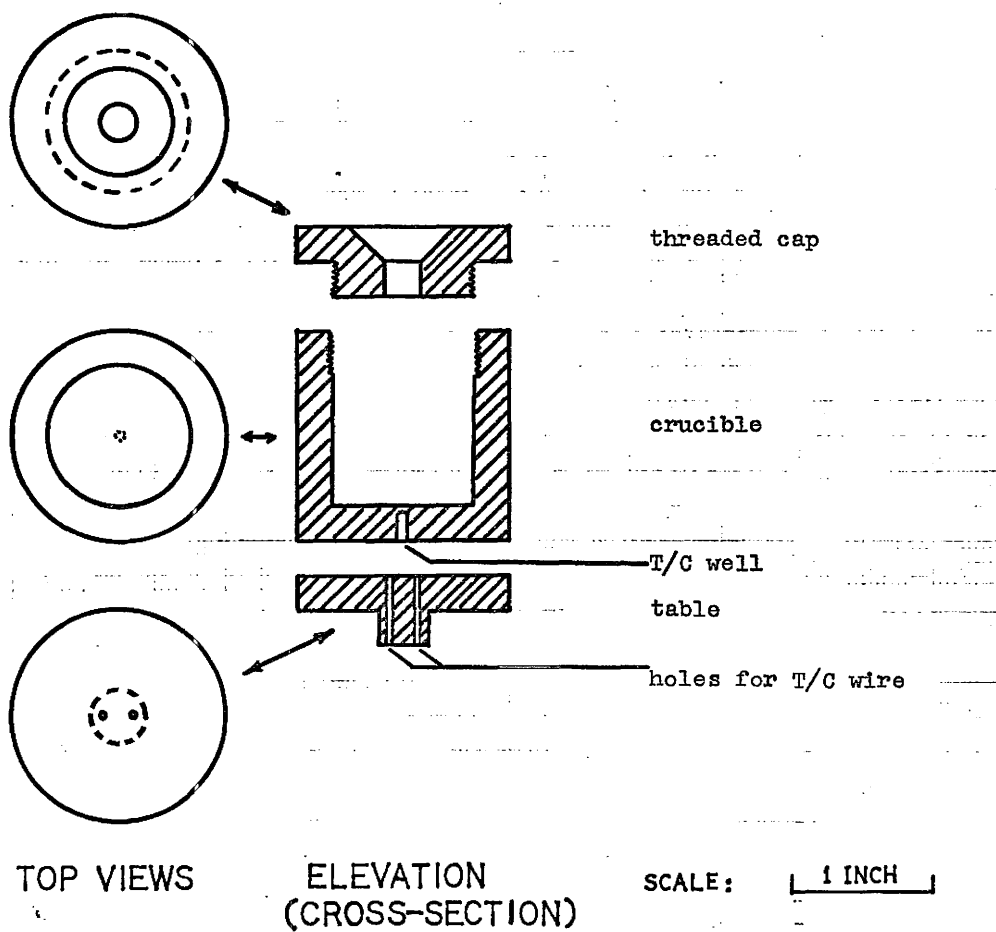
Figure 2.2.2 : Carbon crucible details

wet this material, making it possible to simply dump the leftover charge from the previous evaporation and recharge with fresh material for each run.

The cylindrical filament was constructed of 0.002" thick tantalum foil, available from the A.D. Mackay Co., Garien, Connecticutt. The resistance of the filament was adjusted by cutting an array of holes into the foil before rolling it into its cylindrical form. This was done to increase the filament resistance so that a lower current would be necessary to bring the source to temperature, thereby reducing hot spots in the rest of the source current circuit. The higher the hole density, however, the shorter the filament life became due to thermal stresses in the tantalum foil, and the final design required about 200A to achieve evaporation temperatures. At this hole density (Figure 2.2.3) the filament lifetime is 10 to 20 evaporations, but the high current required, necessitated further design considerations.

First, the isolated high current feedthrough required cooling to avoid separation of the cable from the soldered feed-through connector. This was accomplished using an Edwards 9A watercooled electrode.

Also, 0.5" diameter electrode posts were required to avoid $I^2R$ heating. The current is then fed to the tantalum cylinder with foil strips to maintain a reasonable separation between the hot filament and the electrodes. At first, steel posts and molybdenum strips were used but this lead to problems. The
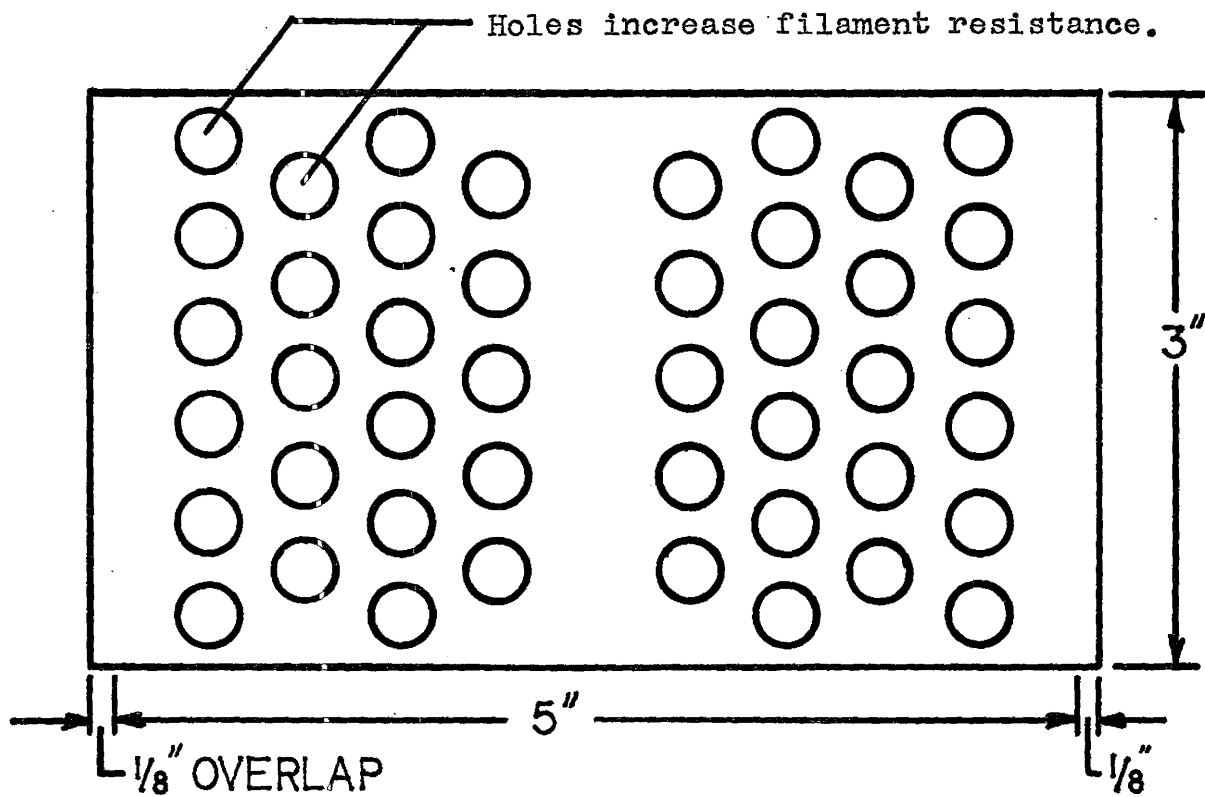
Figure 2.2.3: .002" Ta foil before roll up into cylindrical filament.

steel posts formed a flaky layer during evaporation which broke away from the posts. This threatened to short the post to ground as well as possibly contaminating the evaporant. Subsequent analysis x-ray fluorescence (using SEM) showed the flaky layer to consist of iron and sulphur, probably iron-sulphide. Also, the molybdenum became very brittle and after a few evaporations broke away completely. These problems were solved by using copper posts and contructing the feeding strips of 0.01" thick tantalum, which does not appear to become brittle. The tantalum does not, however, readily weld to copper and an intermediate stainless steel strip was required (see Figure 2.2.4). Because of the high temperature, sulphur rich environment of the source, the surface of the copper rods sulphurized also, forming a silver-grey $Cu_2S$ layer, necessitating a change of posts every 30 evaporations.

Due to the large size of the source, radiant heat during evaporation was a problem, and several layers of heat shielding were used to prevent heating and subsequent sulphurization of the base plate and other surrounding fixtures in the bell jar. Molybdenum foil of 0.002" thickness was available and proved acceptable in the configuration of Figure 2.2.5, with one layer beneath the source, two concentric cylinders around the sides, and 3 layers suspended between source and substrate.

Also, to prevent excessive CdS deposits in the bell jar, a stainless steel shroud was used for evaporant containment (Figure 2.2.5). However, after several evaporations, the CdS films began to take on a very porous and almost powdery texture.

Ta filament

nut

.01" Ta foil

.5" copper electrode

spot welded

stainless steel
    intermediate

stainless steel
    bolt

ELEVATION
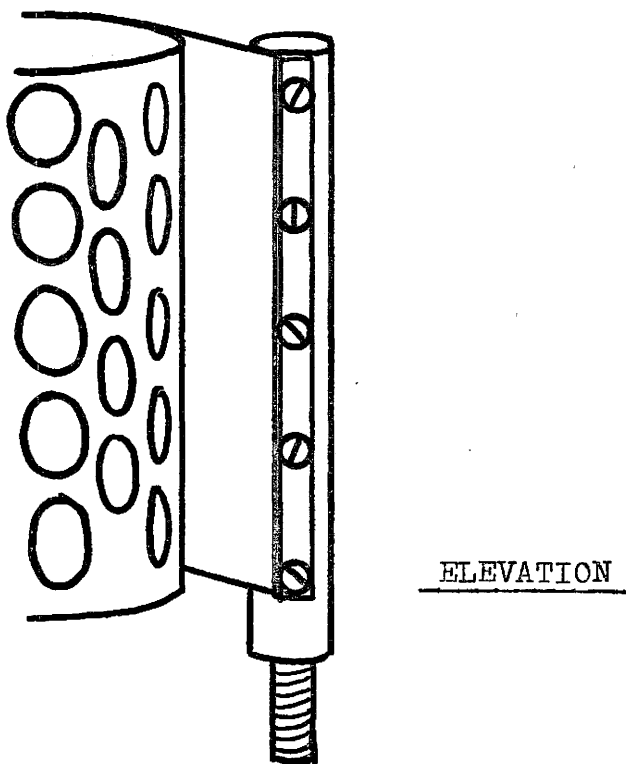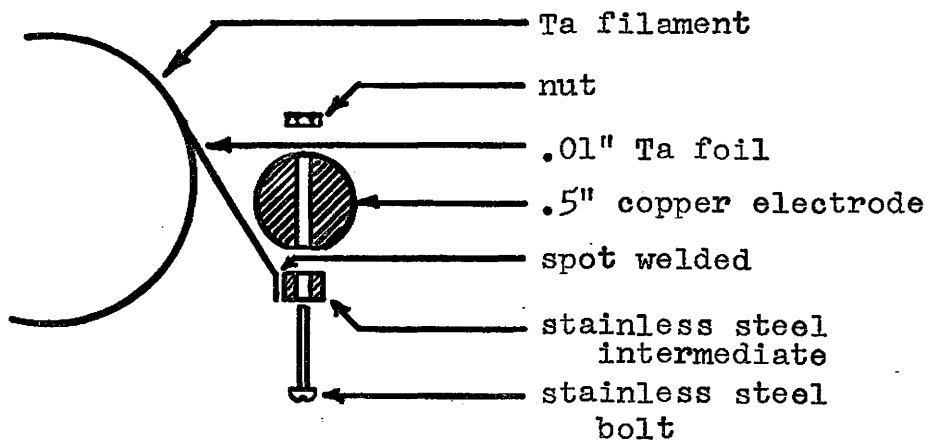
Figure 2.2.4: Filament to electrode post construction
        details.
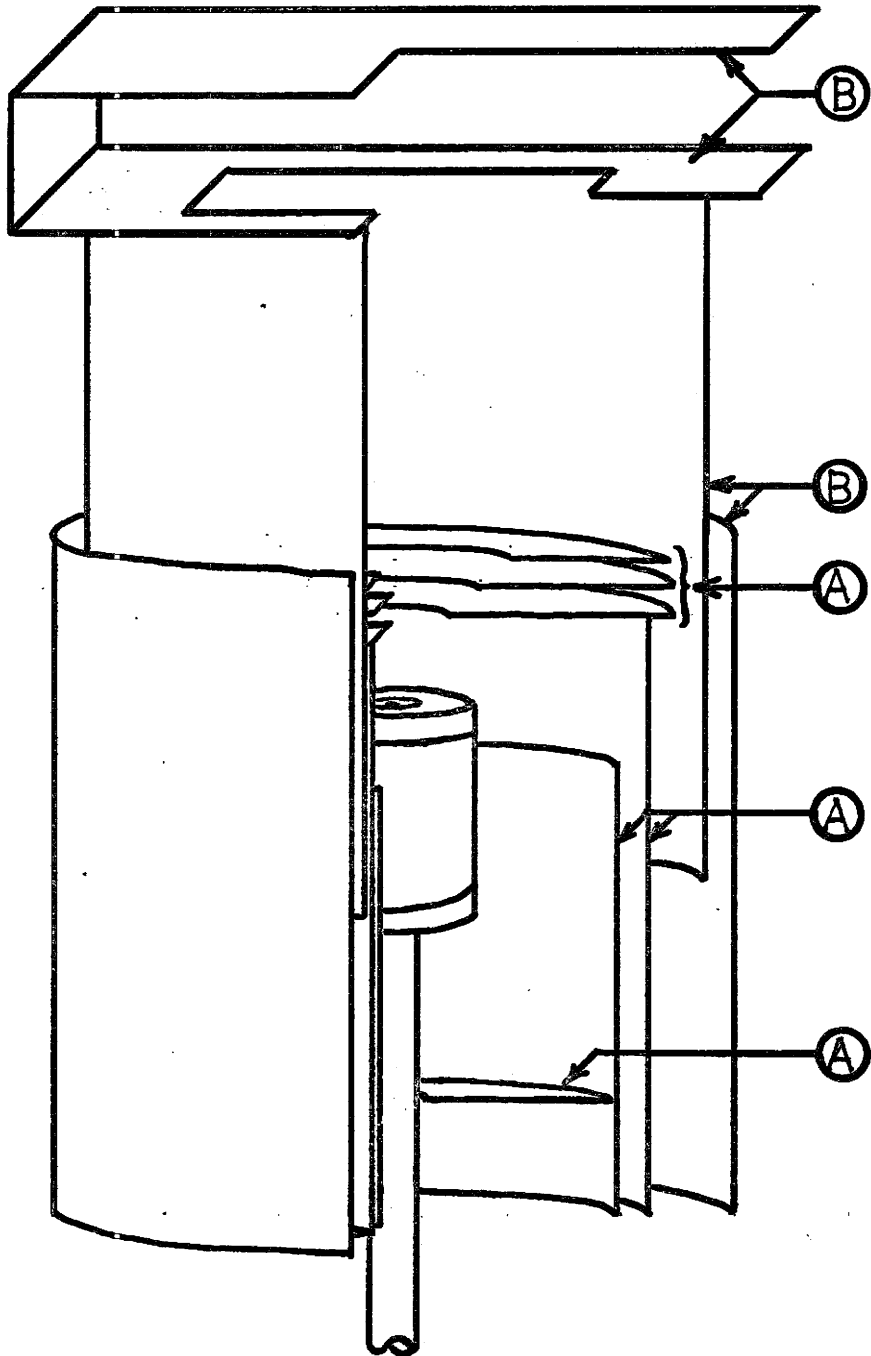
Figure 2.2.5 : Breakaway view of Heat Shielding (A)
and Evaporant Shroud (B) .

It was suggested that sulphur contamination of the diffusion pump had reduced the capacity of the pumping system, and that the powdery nature of the films was due to overpressure in the source. This condition was partially relieved by including evacuation ports in the heat shielding and the shroud, while still maintaining line-of-sight containment. A change of pump oil completely alleviated the problem.

## 2.3  Substrate Assembly Details

As CdS dissociates on evaporation[2], a dynamic equilibrium must be attained between adhesion and re-evaporation at the substrate to maintain a stoichiometric film. Since the adhesion and re-evaporation rates of Cd, S, and CdS vary with temperature[3], and the crystallographic[4], electrical[5], and optical[6] properties of CdS are dependant on the excess Cd content of the film, substrate temperature during evaporation is an important parameter in the preparation of CdS films. According to Wilson and Woods[2], 220°C is the optimum substrate temperature for the preparation of device quality CdS films. With this in mind, a resistively heated substrate assembly was constructed (Figure 2.3.1) to bring the substrates to 220°C for evaporation. However, it was found that the radiant heat from the source was more than enough to maintain high substrate temperatures during the evaporation, and a cooling mechanism was required to maintain control. It was therefore decided to use a water cooled copper block for the substrate mount (Figure 2.3.2). This was
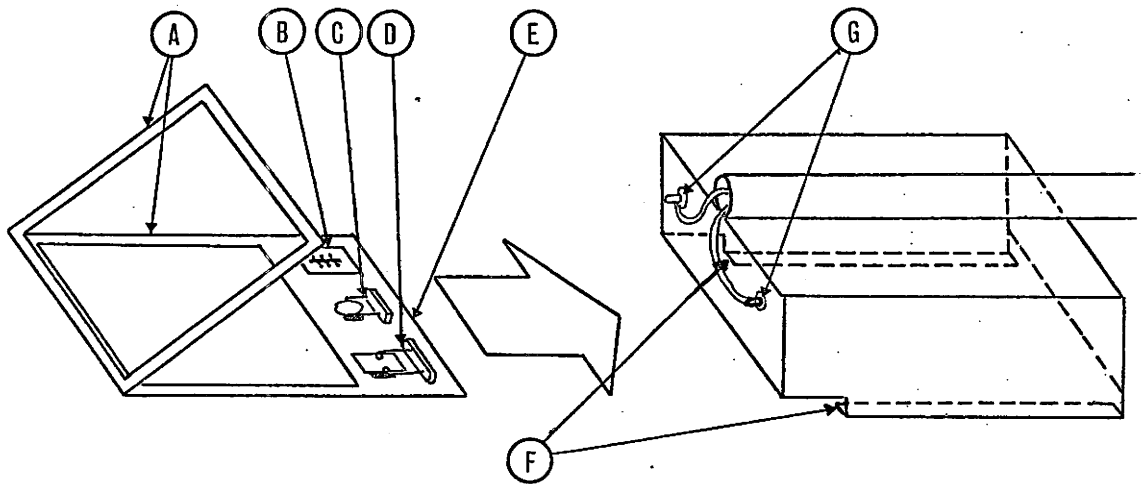
Resistively heated substrate mount showing
large area copper substrate frame (A), test
samples, and monitoring systems (B,C,D).Sub-
assembly (E) fits into heater frame (F),
where heater terminals (G) can be seen.

Figure 2.3.1: Resistively heated substrate mount.

quartz crystal
water cooling
silver solder seal
$\frac{1}{2}$" dia stainless steel
silver soldered
copper block
Al substrate frame

rotary vacuum feedthrough
1/8" stainless steel tubing
flexible tubing
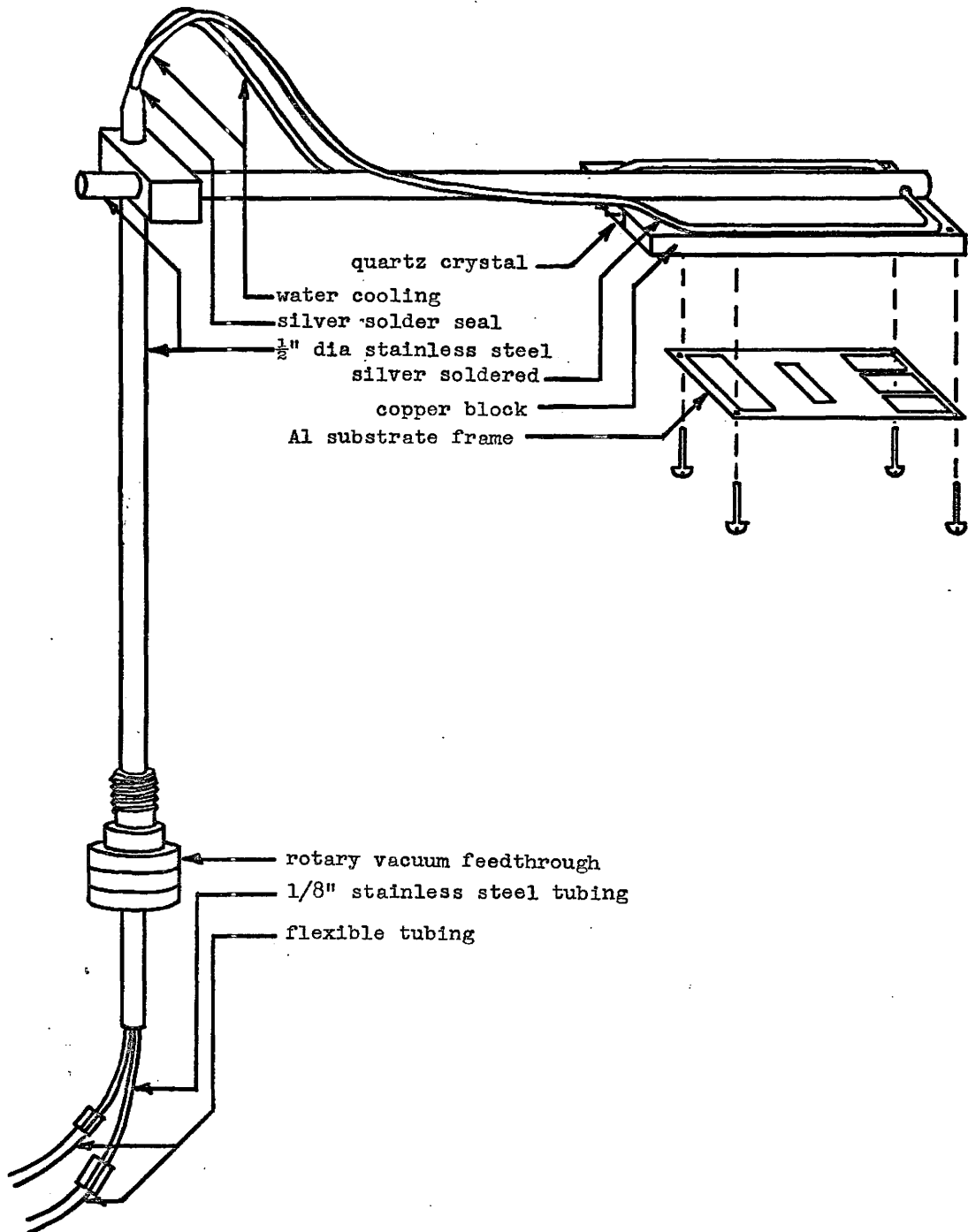
Figure 2.3.2: Water cooled substrate mount.

preheated using the coating unit's radiant heater and water cooled, as required, during evaporation. The large thermal mass of the copper block helped maintain temperature stability.

The CdS evaporation system was designed to be compatible with the dual, in vacuo evaporation of the CdS-$Cu_2S$ heterojunction. For this reason, the substrate assembly was mounted on a mobile carrier, accessible on the outside of the bell jar by means of a double Wilson seal rotary feedthrough. The 0.125" stainless steel tubing for water cooling was connected to flexible nylon reenforced tubing on the outside of the bell jar to allow rotation of the substrate assembly.

Along with the Zn plated copper foil used for the CdS-$Cu_2S$ solar cells, the substrate assembly included several test samples and a quartz crystal for evaporation monitoring. The test samples included a glass microscope slide for optical measurements and x-ray analysis, and a glazed ceramic substrate with pre-evaporated aluminium contacts onto which a Hall bar, defined by a brass mask, was evaporated for electrical characterization of the films (Figure 2.3.3). The 5MHz quartz crystal was used in conjunction with a Sloan Evaporation Monitor to keep track of the deposition while it was in progress. While the system is not calibrated for elevated crystal temperatures, it was felt that a cooled crystal would condense a film from the evaporant stream at a different rate than the heated substrates, and so it was allowed to remain at the same temperature as the substrates. Also, it was found that an increase in cyrstal temperature of 250°C caused a frequency change of only 5 kHz; that is,

Brass mask defines Hall bar
Ceramic substrate with Al contacts
Section of Cu substrate mount

Evaporated CdS film
Glazed ceramic substrate
Pre-evaporated Al contacts
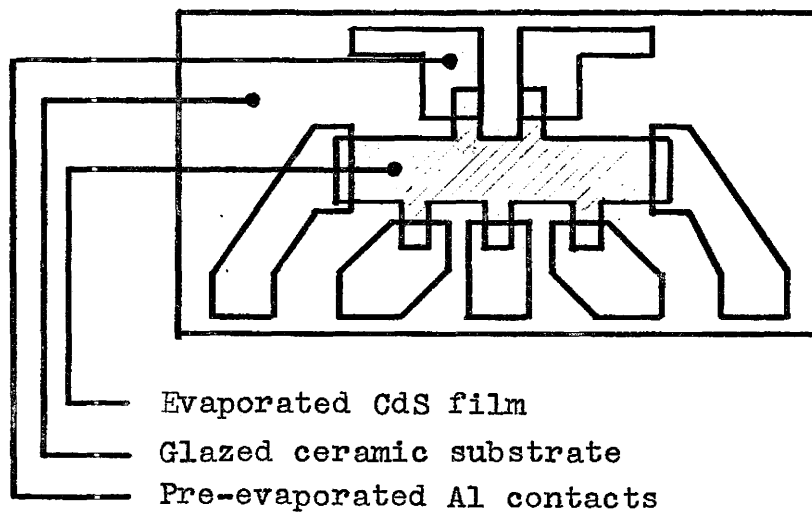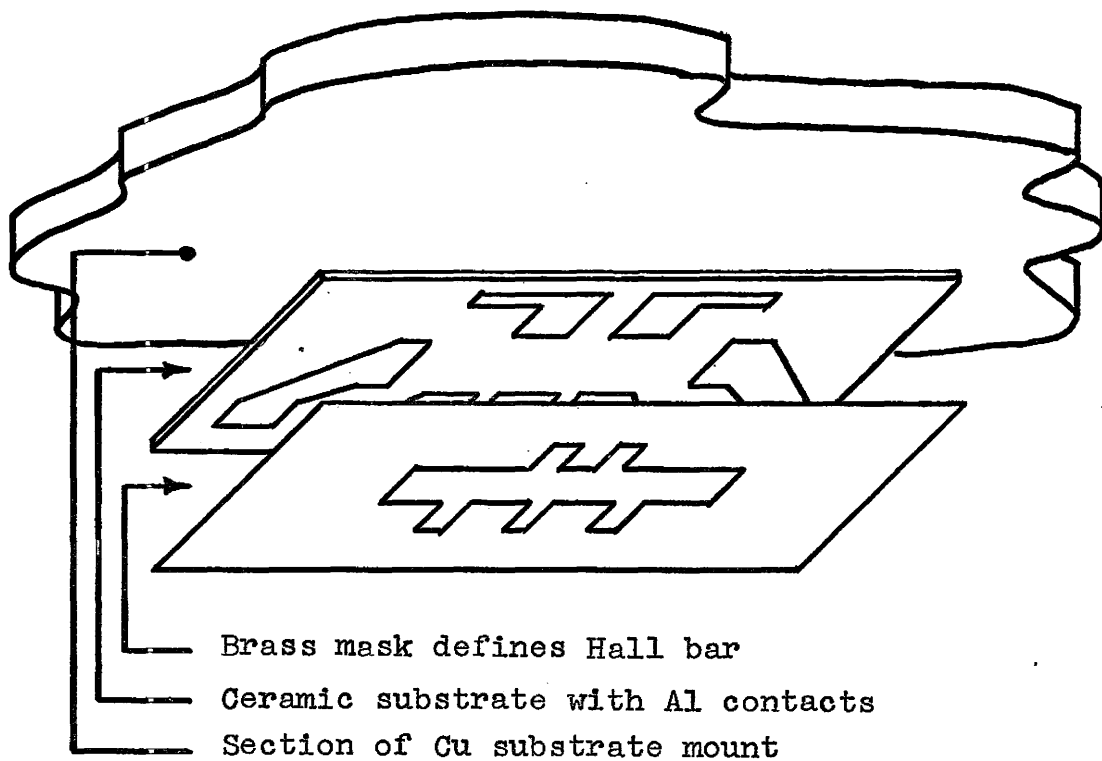
Figure 2.3.3: Hall test bar preparation.

only 5% of the frequency change due to a mass increase from a $4\mu$ thick film. The results from the crystal monitor, then, are taken as read, with an assumed 5% error margin.

## 2.4  System Performance

The major difficulty encountered in the evaporation of the micron thick CdS films is evaporant containment. While line-of-sight shrouding was maintained, dark grey, Cd rich CdS deposits were found on all cool interior surfaces such as the water cooled bell jar wall. Warm surfaces, heated by the radiant heater and by the source, showed yellow deposits, characteristic of more stoichiometric CdS.

There are several reasons why these deposits are unwanted. First, these deposited layers tend to absorb gases during source and substrate reload, and make pump down a time consuming process due to the subsequent outgassing. Second, these conducting layers interfere with electrical monitoring systems such as the crystal thickness monitor and thermocouples. Also, sulphur and/or cadmium contamination of the pump oil was seen to degrade the pumping system's performance as noted earlier.

Of particular interest in the dual system is cross contamination of the $Cu_2S$ source by Cd. Although it has not been determined whether or not this will be significant, it is believed that suitable shrouding of the $Cu_2S$ source arrangement, possibly with a cold wall to condense any possible contaminants, will be

sufficient to maintain a clean $Cu_2S$ evaporation.

Another difficulty encountered is the highly reactive nature of the hot sulphurous environment around the source during evaporation. Because of this, the materials to be used for source construction were limited. The molybdenum heat-shielding performed well, showing no appreciable deterioration after fifty evaporations. For the cooler shrouding, stainless steel was found to be acceptable. For the larger volume source current electrodes, however, the cost of molybdenum or tantalum would have been prohibitive, and a compromise had to be made. Copper was used as much as possible, since the sulphurized outer layer remained an integral part of the structure, but the replacement of high conductivity copper by semiconducting $Cu_2S$ made electrode replacement necessary every 20 to 30 evaporations.

The films produced by this system seem to be appropriate for the use in $CdS-Cu_2S$ solar cells and the control of substrate temperature allows adjustment of film properties and hence optimization of the cell's performance. It is felt, however, that the source arrangement is slightly larger than necessary, and that scaling down by a factor of about 3/4 would still provide adequate CdS charge volume for $10\mu$ to $20\mu$ films, and would increase the life of the structure to more acceptable limits for production.

## 2.5 Proposed Dual CdS/Cu$_2$S Evaporation

The best results to date for the Cu$_2$S on CdS heterojunction solar cell have been obtained using the dip process wherein the evaporated CdS film is dipped in a CuCl solution and the surface layer of the CdS is converted to Cu$_2$S by an exchange reaction. It is thought that the primary advantage of this process is that the junction is formed within the CdS material; that is, in a region unexposed to environmental contamination. On the other hand, the double evaporated structure puts the junction at the CdS surface where possible contaminants may disrupt barrier formation at the interface. In the proposed double evaporation in vacuo system, where the Cu$_2$S layer is deposited in the same apparatus as the CdS layer without leaving vacuum between operations, this problem should be eliminated by maintaining a clean CdS surface.

As indicated earlier, the present CdS evaporation apparatus was designed to be compatible with the dual source system. The large vacuum chamber of the Edwards 19E6 coating unit has enough space for the two shrouded sources, and the substrate mount was designed in a mobile configuration (Figure 2.3.2) to allow the substrate to move from one source to the other. It was decided to use a mobile substrate rather than the rotating multiple source provided by Edwards so that suitable shrouding could be used on both sources to avoid cross contamination. Figure 2.5.1 shows a plan view of the proposed set up. Included in the design are

CDS SHUTTER

CDS SOURCE

MOBILE SUBSTRATE ASSEMBLY

BELL JAR INNER WALL

WORK PLATE

$CU_2S$ SOURCE

$CU_2S$ SHUTTER

**TOP VIEW**

SUBSTRATE
SHUTTER

SOURCE

**ELEVATION**

OF SINGLE SOURCE

SCALE ⊢ 1 in. ⊣

TO PUMP
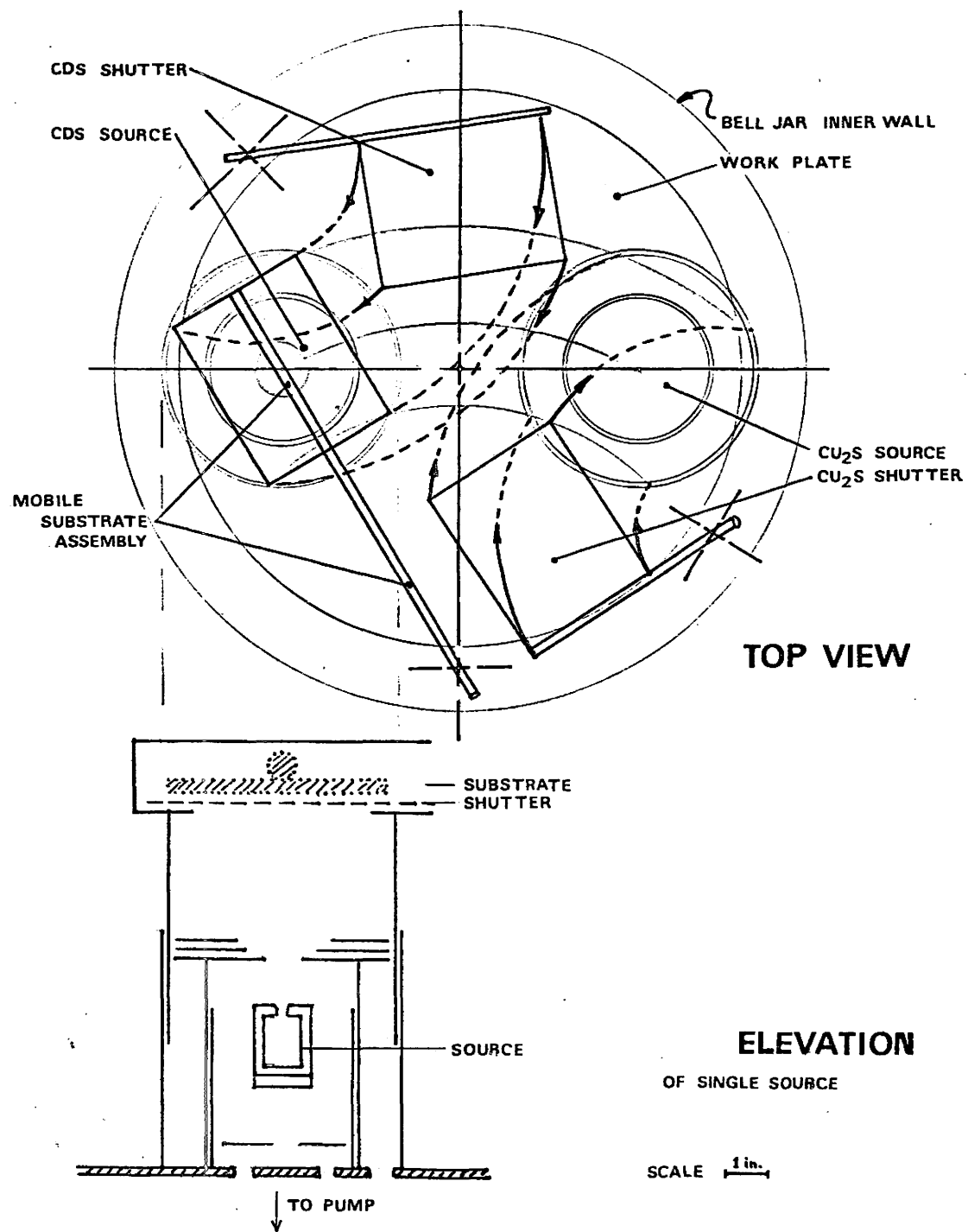
Figure 2.5.1 : Proposed Dual $Cu_2S$-CdS Evaporation System.

dual shutters to help prevent contamination by sealing in completely the source not in use.

Due to the amazing ability of CdS to evade containment, however, it may be necessary to use water cooled shrouds. This would preferentially condense the evaporant away from the other source, but would necessitate more frequent cleaning of the apparatus due to excess film build up, and will be included only if necessary.

# SECTION 3

## EXPERIMENTAL RESULTS AND DISCUSSION

### 3.1 Introduction

As the number of variables to be observed was so high, efforts were confined to confirming film behaviour as reported in the literature, and determining how well the system as previously described performed in comparison with other evaporation systems.

Of prime concern, apparently, is the stoichiometry of the CdS, and how it can be adjusted by varying source temperature and substrate temperature. A brief investigation of the evaporation kinetics of CdS by Wilson and Woods[2] indicates that for substrates above room temperature, no free sulphur should exist in the deposited films, and as the substrate temperature increases the free cadmium content decreases. On the other hand, for increasing source temperatures, the free cadmium content increases. This free cadmium has several effects on the film's properties as is discussed below.

The crystallographic properties of the film are also important, as shown by Kazmerski et al[5] who found that for a well oriented film (i.e. c-axis perpendicular to the substrate) the electrical properties are anisotropic making it necessary to distinguish between in-plane ($\perp$ c-axis) and cross-plane ($\parallel$ c-axis) properties. As grain size and degree of orientation depend on

deposition rate and film thickness, these variables must be considered as well.

The above properties are discussed in more detail in the following sections.


## 3.2 Optical Properties

The effects of free Cd on the optical properties of CdS have been noted by several authors. Kuwabara[7] attributes the weak absorption to long wave lengths and the resulting orange colour of his films to free cadmium. Wendland[6] presents transmission versus wavelength for varying source temperature and substrate temperature. While he does not specifically refer to free cadmium, if it is assumed that the cadmium vs. temperature relationships presented by Wilson and Woods[2] hold, Wendland's curves show increased absorption and a less distinct absorption edge with increased cadmium content.

Typical optical data for CdS films prepared in this study are shown in Figure 3.2.1. These films were produced with a substrate temperature of 220°C and a source temperature of 1000°C. A very strong absorption edge at 2.4 eV can be seen in the transmission curve, agreeing well with the published value for the CdS bandgap at 2.42 eV.[8] The oscillations in both curves for $\lambda > .7\mu$ are due to interference effects produced by multiple reflections in these smooth films. The positions of the maxima for reflection can be determined by the equation:[9]

Figure 3.2.1 : Experimentally determined Transmission and Reflection of two evaporated CdS films as a function of wavelength.

26
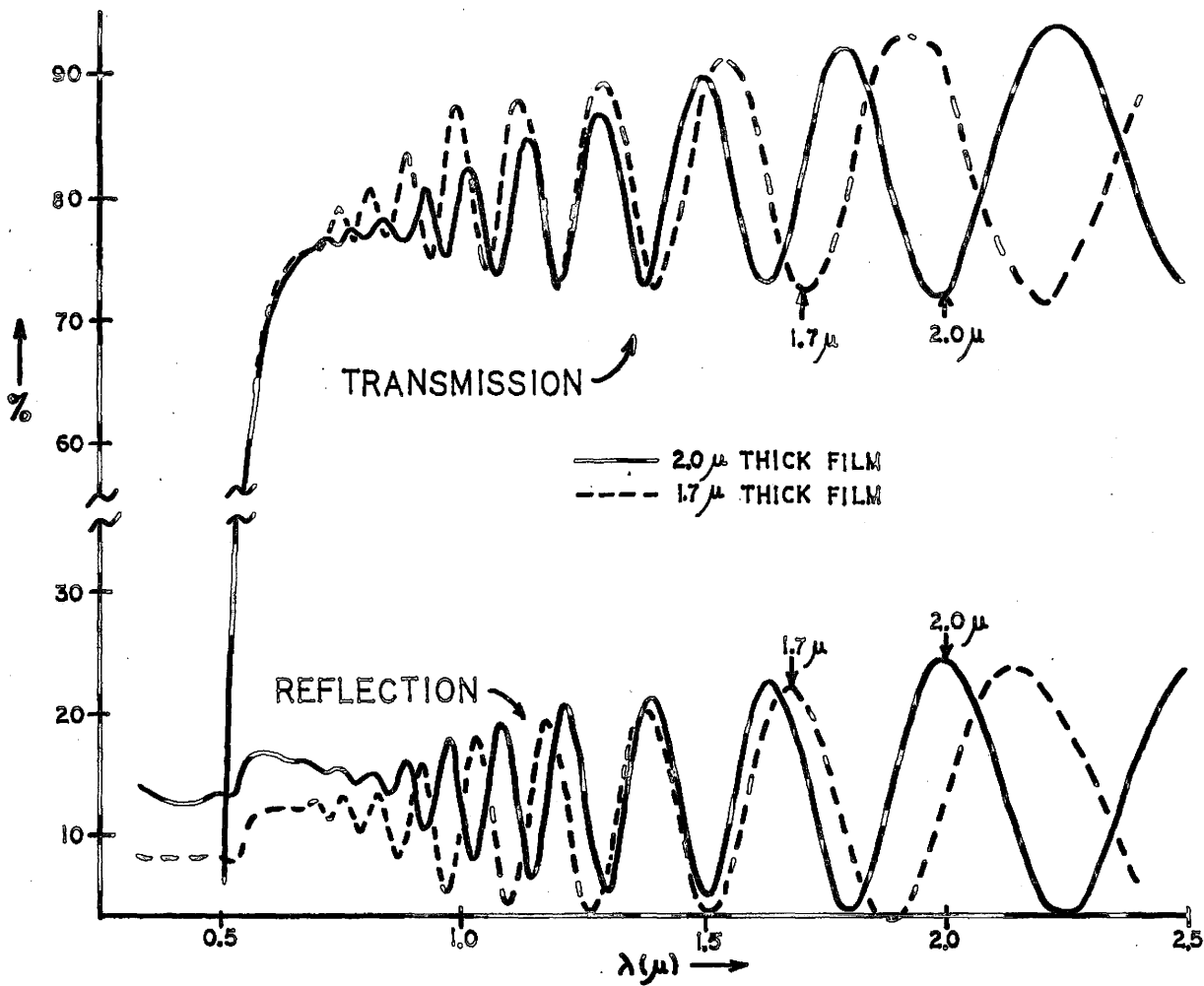
$$2nd = (m + \tfrac{1}{2})\lambda$$

where n is the refractive index of the films, d, the film thickness, m, an integer, and $\lambda$, the light wavelength. By extrapolation of the data presented by Bieniewski and Czyzak[10], the index of refraction, n, of CdS for a wavelength of $2\mu$ would be about 2.25, which, when substituted into the above equation, accounts for the peak near $\lambda = d$.

## 3.3  Crystallographic Results

Several CdS source materials as well as many of the evaporated films were studied using x-ray diffraction with nickel filtered Cu K$\alpha$ radiation at $\lambda = 1.542\overset{\text{o}}{\text{A}}$. The film test samples were evaporated onto cleaned microscope slides, at a rate of 2500 $\overset{\text{o}}{\text{A}}$/min, to a thickness of about $10\mu$.

The source materials considered include a commerical grade of CdS powder from Fisher Scientific, two types of sintered electronic grade powder from General Electric (GE 118-8-2 and GE 118-8-16(X-137)) and single crystal chips of ultra-high purity from Eagle Picher. The two GE materials and the Eagle Picher chips showed $\alpha$CdS (hexagonal) spectra. The Fisher material however is predominantly $\beta$CdS(cubic). How this effects the resultant evaporated film was not determined as the Fisher material was rejected due to its high impurity levels. These impurities include (from the Fisher prepared assay): Cl ($1.6 \times 10^{19}$ cm$^{-3}$), Pb ($1.4 \times 10^{18}$ cm$^{-3}$), Zn ($4.4 \times 10^{17}$ cm$^{-3}$), As ($3.9 \times 10^{17}$ cm$^{-3}$),

and $Cu(2.3 \times 10^{16} \text{ cm}^{-3})$. Typical x-ray spectra of the source

materials are shown in Figure 3.3.1, with published[11] spectra

for $\alpha$CdS and $\beta$CdS included for comparison.

Typical x-ray results for the evaporated films are shown

in Figure 3.3.2. Without exception, the films were all $\alpha$CdS with

a strong c-axis orientation indicated[12,13] by a (002) 100%

peak at d = 3.36Å and (004) 1 to 2% peak at d = 1.68Å. Attempts

were made to produce randomly oriented slurries of the evaporated

films by scraping the CdS from the glass substrates and dropping

a small amount of acetone on a pile of the resulting powder.

However, the spectra from these slurries were also characteristic

of c-axis oriented films with a few < 1% peaks showing up due to a

slight decrease in alignment. It is thought that the platelets

scraped from the glass were large enough to resettle in the

same orientation as in the original film.

X-ray spectra of films produced at three substrate

temperatures (200°C, 120°C, 70°C) were also taken. Visually,

the 200°C film was clear yellow, the 120°C film was clear orange,

and the 70°C film was dark brown. The x-ray spectra showed a

slight decrease in aligned orientation as the substrate temperature

was decreased. This was seen in the appearance of more peaks

besides the (002) and (004) although these latter two remained

dominant. It is also interesting to note that the 70°C film

spectrum included a 0.1% peak corresponding to the 100% (101)

free cadmium peak at 2.34Å and a 0.06% peak (barely above noise level)
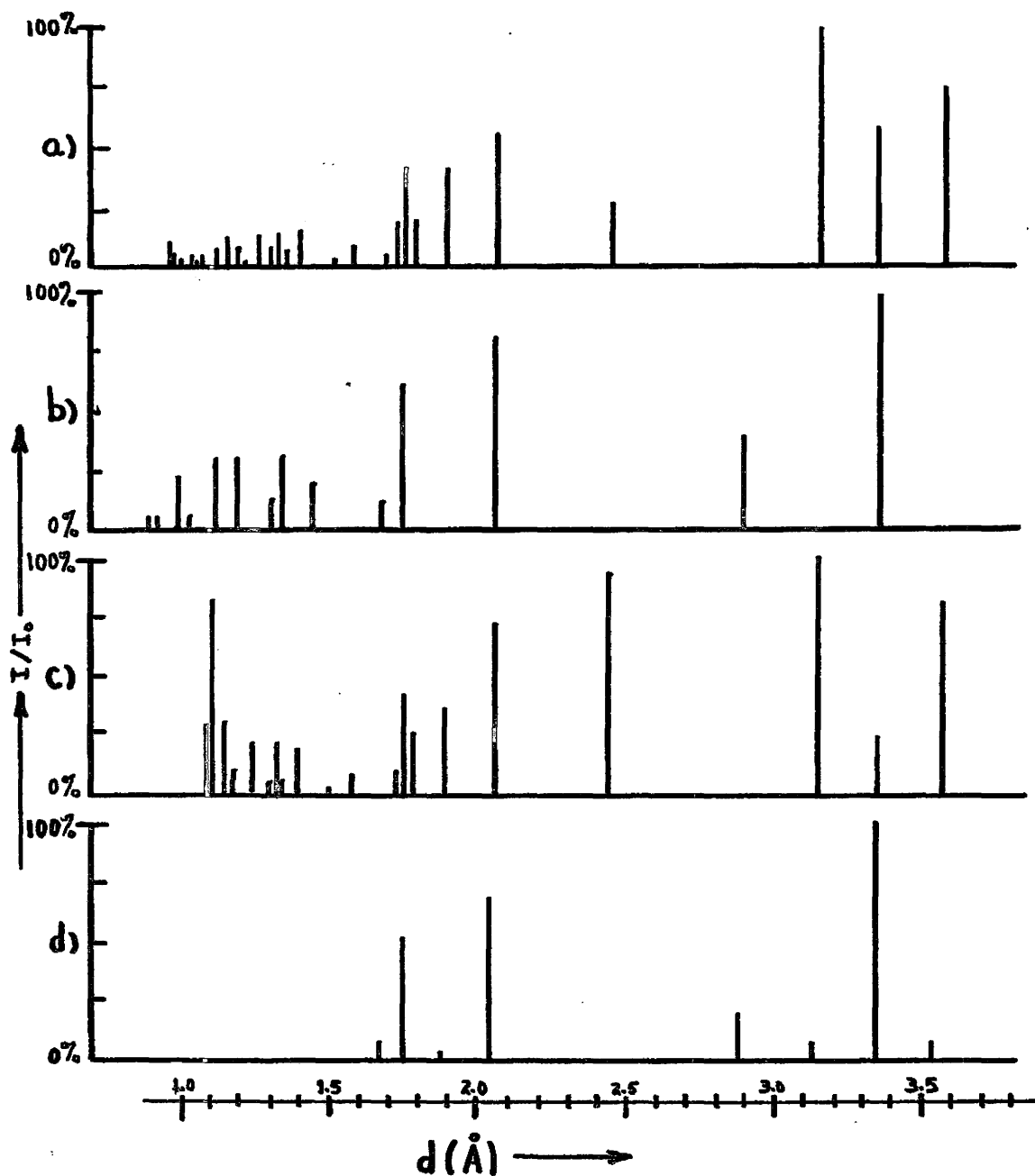
Figure 3.3.1 : X-Ray Spectra of Hexagonal ∝CdS (a) and
Cubic βCdS (b) are compared with Spectra
for GEll8-8-16 powder (c) and Fisher
CdS powder (d) .
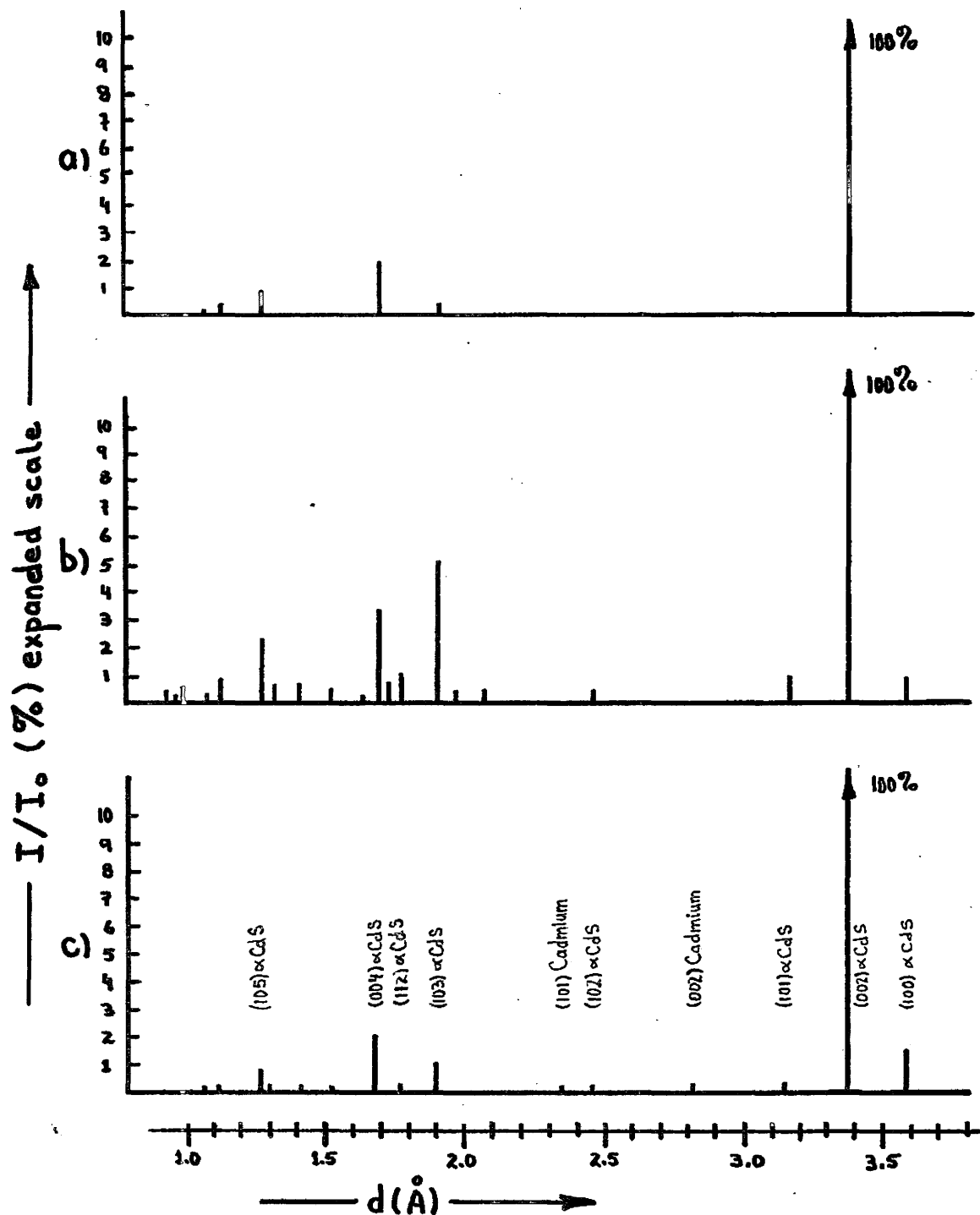
Figure 3.3.2 : X-Ray Spectra of (a) Evaporated film,
(b) Slurry of material scraped from
evaporated film, and (c) film with
substrate temperature < 100° C. Indices
of primary refraction planes are given
in (c) .

at the 65%(002) Cd location 2.81Å. This confirms the presence of

free cadmium in the low substrate temperature evaporated film as

indicated in the literature[2].

## 3.4  Electrical Characteristics

As the CdS films prepared are to be used in the manufacture

of photovoltaic cells, the electrical characteristics of the films

and the control of these properties are of utmost importance to

allow for the optimization of the resultant solar cells. The

electronic properties of CdS films have been investigated by

several authors[2,4,5,7,14,15,16], and the object of this report

is to verify that the present system behaves according to the

reported trends.

Carrier concentration and type, resistivity and mobility

for the evaporated films were determined using a six point Hall

test bar as shown in Figure 2.3.3. The bars were evaporated through

a metal mask onto glazed ceramic substrates with pre-evaporated

aluminium contacts. All samples were evaporated at a rate of

2500 /min. to a thickness of between 5 and 10 microns. The CdS

to aluminium contacts were found to be low resistance and ohmic.

As CdS has a large photoconductive response, all measurements

were made after the sample had been mounted in an evacuable chamber

and dark for several hours. All films were invariably n-type with

concentrations of $10^{16}$ cm$^{-3}$ to $10^{20}$ cm$^{-3}$ and resistivities of from

0.19 Ωcm to 100 Ωcm. Carrier mobilities ranged from 0.4 cm$^2$/v.s

to 8 $cm^2$/v.s.

The test configuration of Figure 3.4.1 yields[8]:

$$R_H = \frac{E_y}{J_x B_z} = \frac{V_H t}{IB} = \frac{-r}{qn}$$

where $V_H$ is the measured Hall voltage in the y-direction, t, the sample thickness in the z-direction, r, the scattering parameter, and n, the carrier concentration. In the automated apparatus used[17], I is adjusted to keep the voltage drop across the x-direction, $V_C$, at about 1 volt. Therefore:

$$I = \frac{V_C}{resistance} \approx 1 \times (\frac{wt}{\rho \ell})$$

where w, t, and $\ell$ are the sample dimensions and $\rho$ the resistivity of the sample. Then:

$$V_H = \frac{R_H IB}{t} \approx \frac{R_H}{\rho} \cdot \frac{wB}{\ell} = \mu_H \frac{wB}{\ell}$$

where $\mu_H$ is the Hall mobility and is equal to the carrier mobility, $\mu$, times the scattering parameter, r. If r is set to unity, $\mu = \mu_H$.

Practical samples generally behave more like that shown in Figure 3.4.2, where the offset in Hall contacts is due to mask misalignment, film nonuniformities or contact difficulties. Hence, the measured Hall voltage, $v_H$, includes the actual Hall voltage, $V_H$, plus an offset conductivity component due to the displacement, d, along the x-axis from one Hall contact to the other:

$$v_H = V_H + \Delta V_C = V_H + \frac{d}{\ell} V_C \approx V_H + \frac{d}{\ell}$$
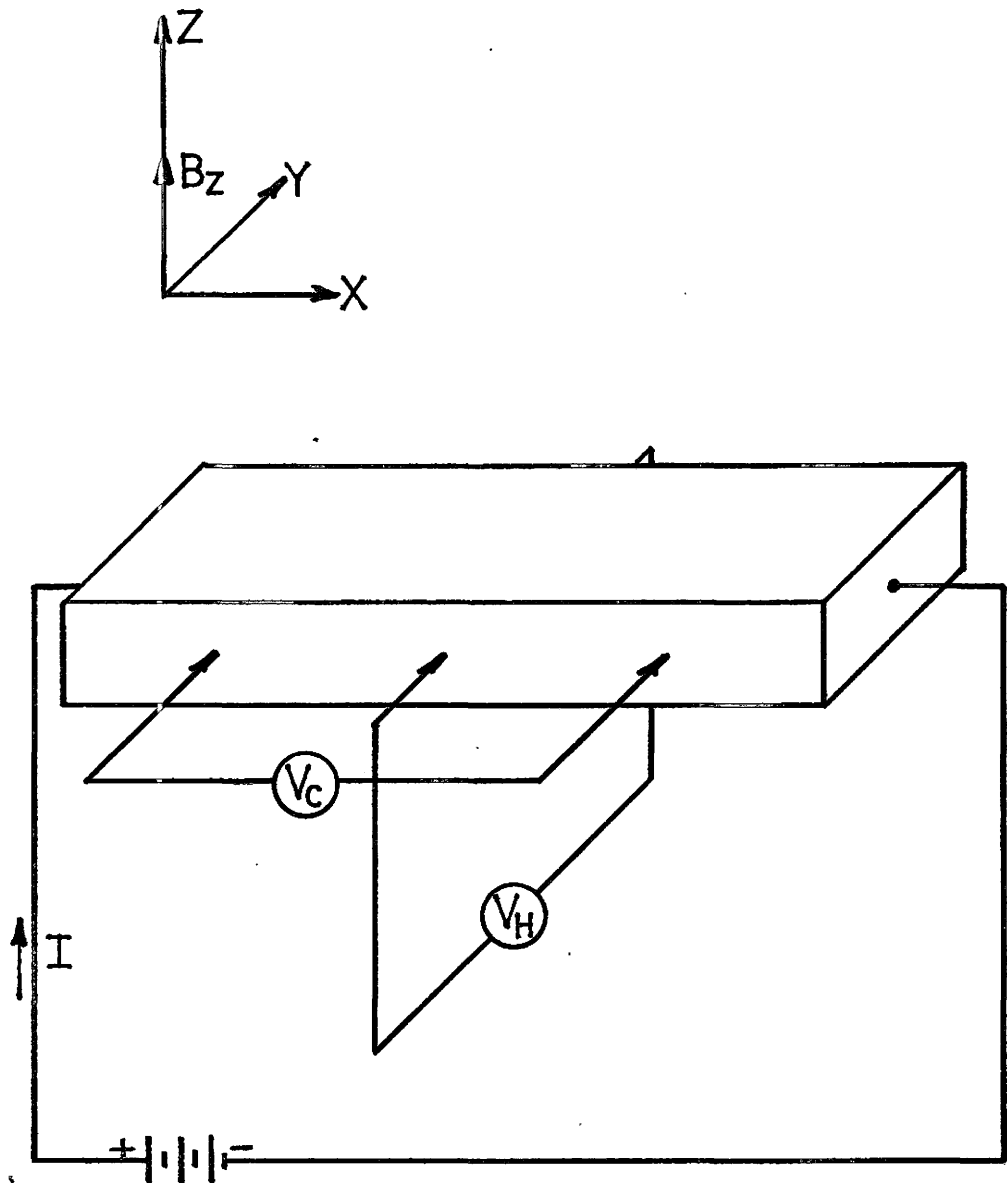
Figure 3.4.1: Six point Test Bar showing Hall voltage, $V_H$, and Conductivity voltage, $V_C$.
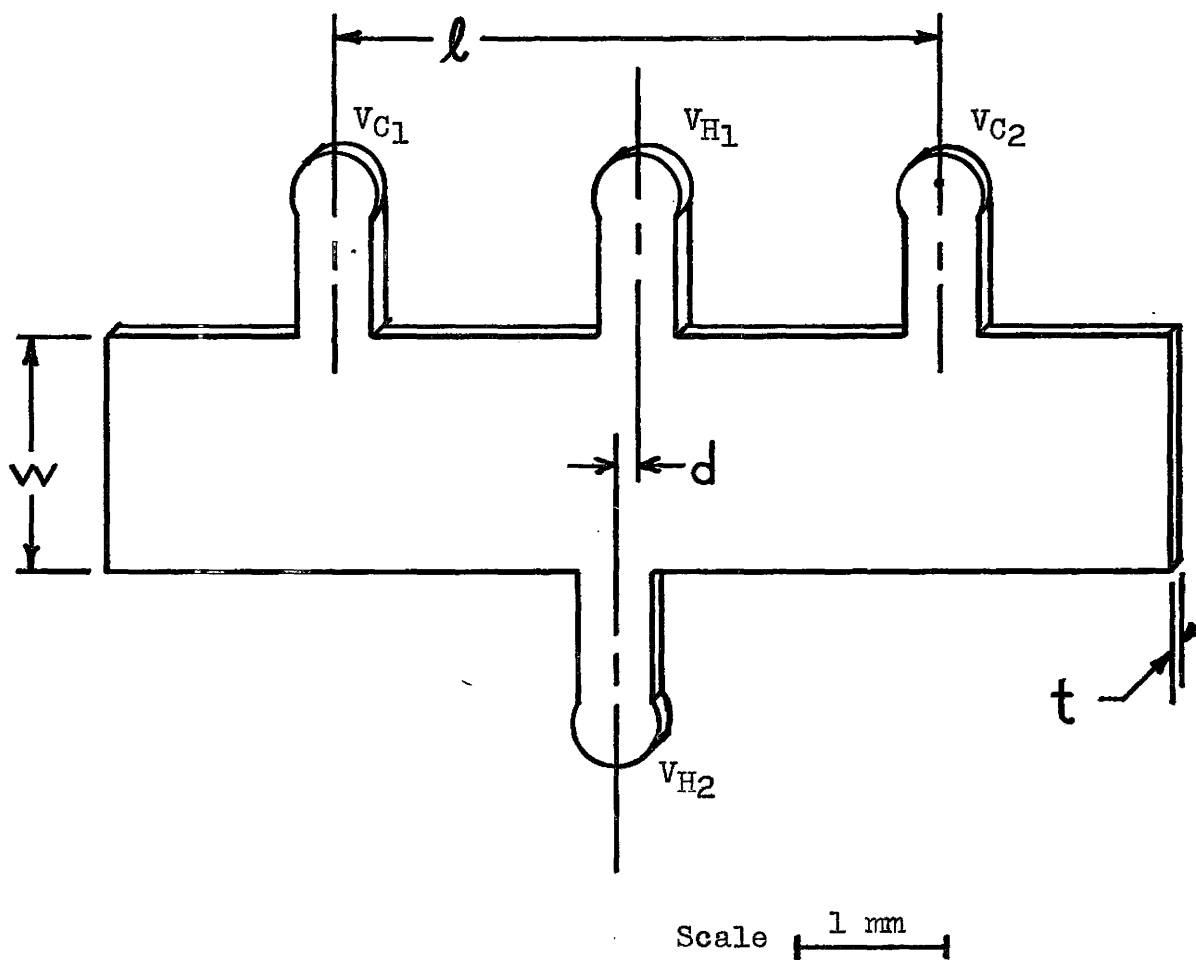
Figure 3.4.2 : Practical Hall test bar showing
offset causing conductivity component
to be added to the Hall voltage.

For low mobility samples, then:

$$V_H = \mu_H \frac{wB}{\ell} V_c = (1 \frac{cm^2}{v.5})(\frac{.15 \ cm}{.5 \ cm})(10^{-4} \frac{v.5}{cm^2})(1v) = .3 \ mV$$

That is, typically $V_H$ is 0.03% of $V_c$. Therefore, in order to see $V_H$ accurately, $d/\ell$ must be less than 0.03%. This is not possible, so an alternate zeroing method was tried. Samples were prepared in the modified configuration of Figure 3.4.3, which has two $V_H$ contacts on one side, a and b. In this case, a to $V_{H_1}$, has a negative conductivity component, and b to $V_{H_1}$, positive. The two potentiometers in the figure can be used to set $V_{H_2}$ to $V_{H_1}$ to zero under zero field conditions $(V_H \propto B = 0)$, which in effect, sets $d/\ell$ to zero and $v_H = V_H$.

While this modification has substantially reduced the offset in $v_H$, it cannot be zeroed, and for very low mobility samples $(\mu = 0.2cm^2/v.s)$ the noise level in $V_H$ produces a large error in $n \propto 1/v_H$.

This high error in concentration is seen in Figures 3.4.4 and 3.4.5 where n is plotted versus substrate temperature and source temperature respectively. Here, general trends can be seen to indicate that the excess cadmium noted in the x-ray evaluations act as donor impurities, but the error margin makes the data inconclusive.

Of particular interest however, is the cold substrate (70°C) film in Figure 3.4.4 whose carrier concentration is substantially higher than the 200°C substrate films. This is the same film in which the x-ray analysis showed small free cadmium peaks (Figure 3.3.2).
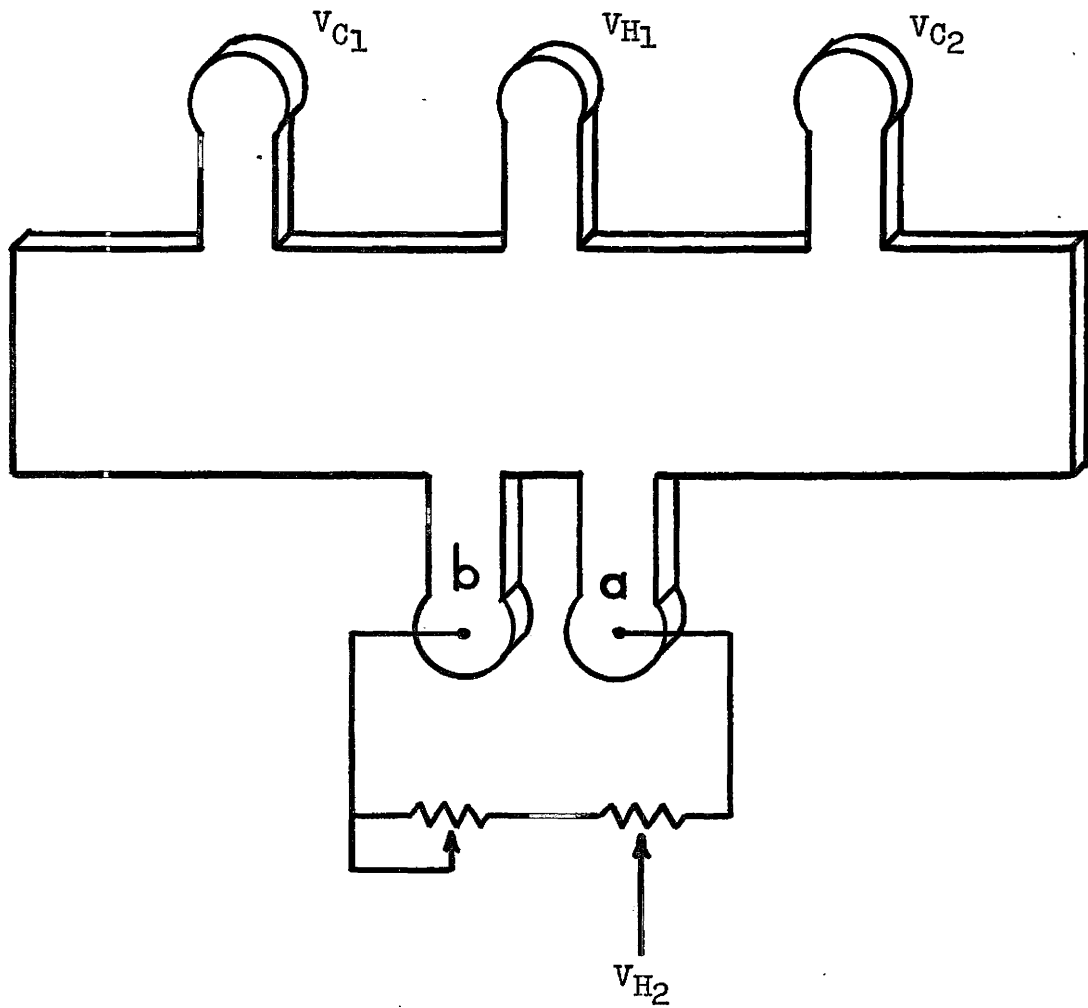
Figure 3.4.3: Modified Hall test bar with provision
for nulling of $V_H$ .
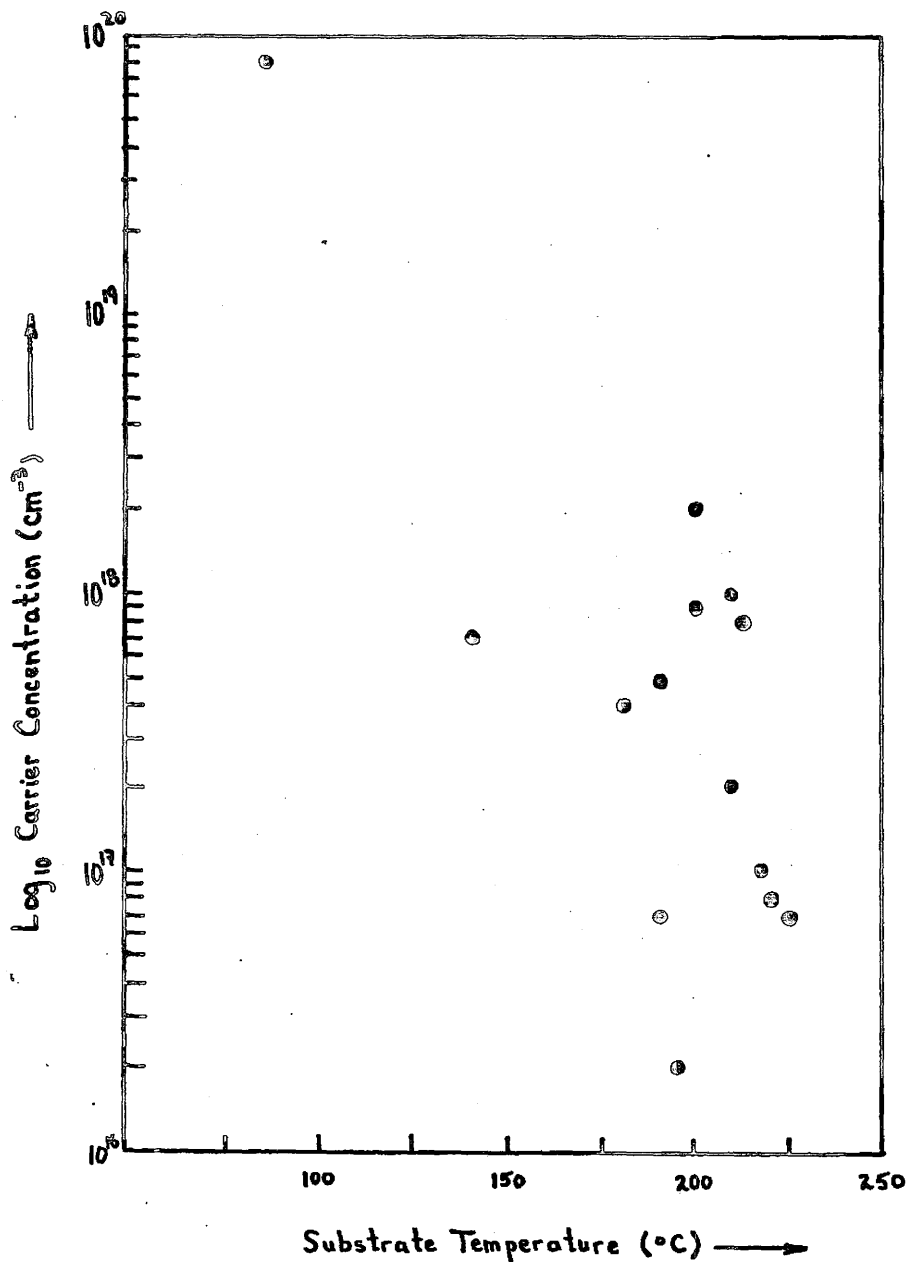
Figure 3.4.4 : Log Carrier Concentration vs. Substrate
Temperature for evaporated CdS films.
(Source Temperature was 1050°C)
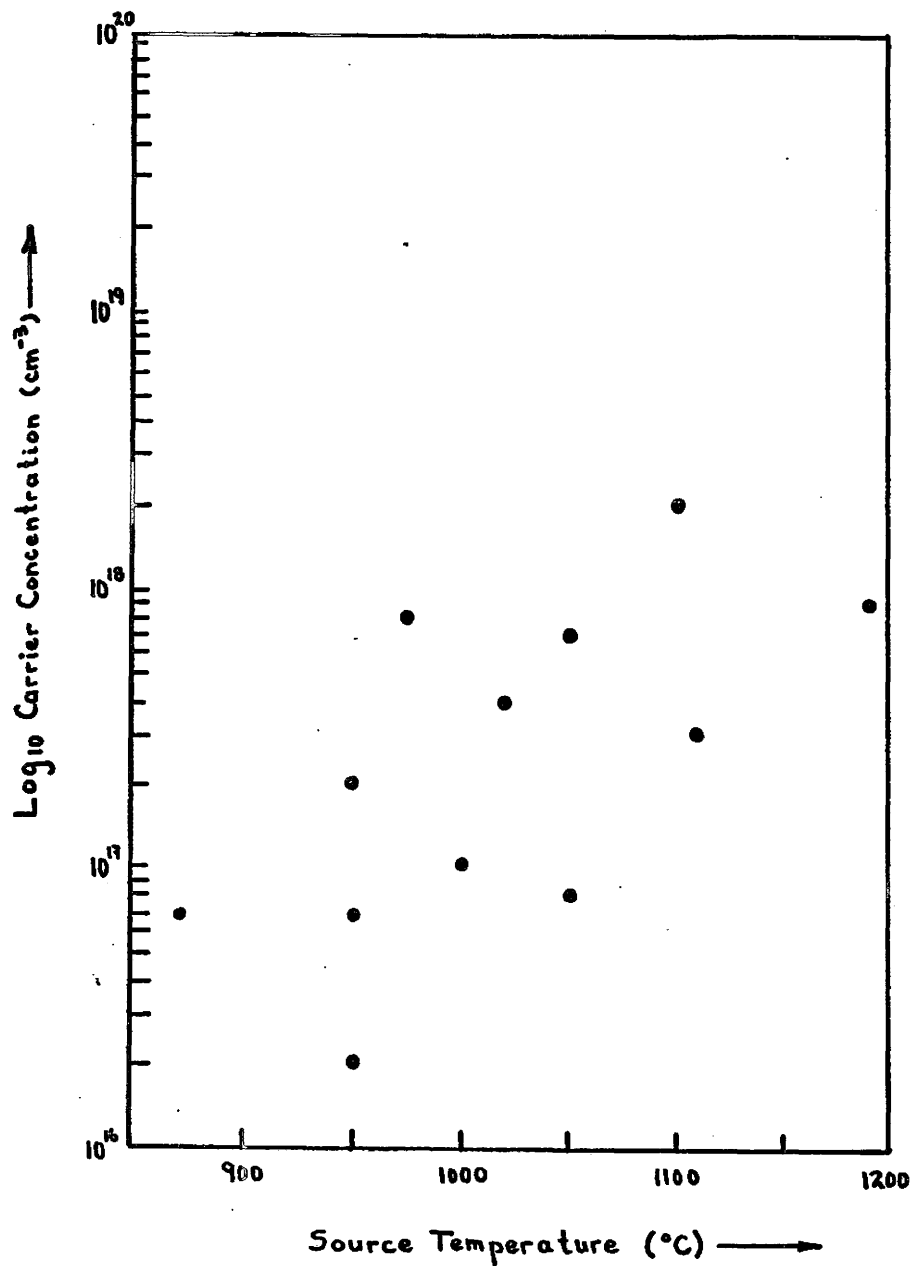
Figure 3.4.5 : Log Carrier Concentration vs. Source
Temperature for evaporated CdS films.
(Substrate Temperature was 200°C)

The resistivity measurements, made essentially using a four-point method with the test bar of Figure 3.4.3, did not have these noise problems. Figure 3.4.6 and 3.4.7 show log ρ versus substrate temperature and source temperature respectively. The results here are quite conclusive.

Assuming again that the excess cadmium atoms act as donor impurities, the analysis of Wilson and Woods (see section 3.1) suggests that for increasing substrate temperature, the free cadmium content should decrease, and hence the resistivity should increase. This was indeed found to be the case as shown in Figure 3.4.6. Similarly, an increase in source temperature should result in a decrease in resistivity due to the excess cadmium, and this behaviour is also confirmed as shown in Figure 3.4.7.
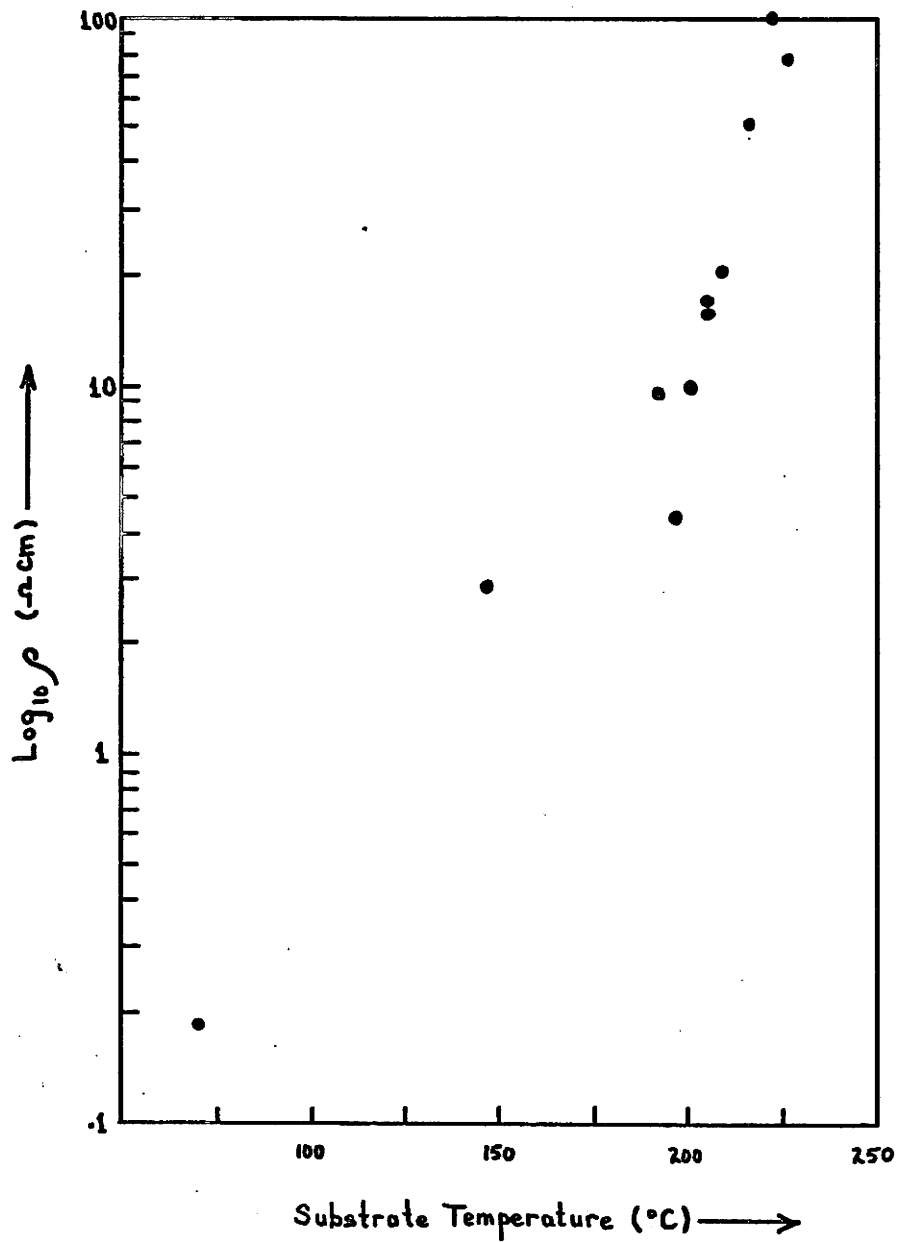
Figure 3.4.6 : Log Resistivity vs. Substrate Temperature.
(Samples as in Figure 3.4.4)
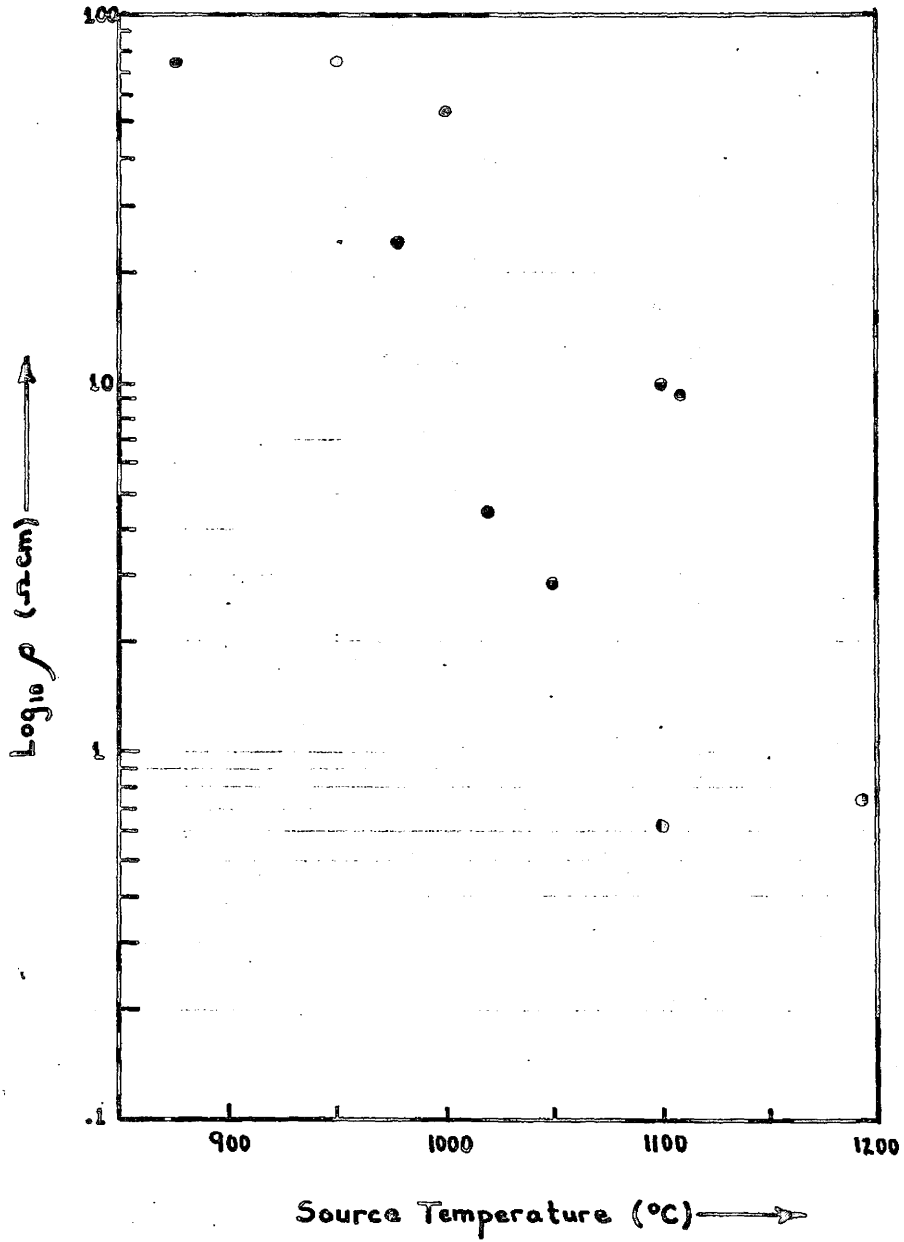
Figure 3.4.7: Log Resistivity vs. Source Temperature.
(Samples as in Figure3.4.5)

# SECTION 4

## SUMMARY

A $Cu_2S$/CdS dual in a vacuo evaporation system, with complete source shrouding and mobile substrate assembly was designed. The CdS half of the apparatus was constructed and proved functional. Because CdS dissociates on evaporation, the kinetics of the deposition must be considered and controlled. Thermal control of the source and substrate was included for this purpose. Chromel-Alumel thermocouples were used for both temperature measurements, and control was maintained manually be adjusting electrode current in the case of the source, and by water cooling to reduce the radiant heating of the substrate by the source.

The concept of free cadmium as the doping mechanism in CdS is a workable idea, and explains the observed variation of film properties with substrate and source temperature. By controlling these temperatures, the electrical, optical and crystallographic properties of the CdS films can be tailored to optimize the photovoltaic response of the $Cu_2S$/CdS cell. Resistivities of 0.2 to 100 $\Omega$cm and carrier concentrations of $2 \times 10^{16}$ to $9 \times 10^{18}$ $cm^{-3}$ have been achieved. Doping and post evaporation treatments as discussed by several authors[18,19,20] have not been considered.

It is hoped that use of the dual evaporation scheme, and adjustment of CdS properties will lead to the development of an inexpensive and easily fabricated solar cell.

# REFERENCES

1.  Reports #1 to #4 on D.S.S. Contract No. 11SQ31042-6-8142, Serial #1SQ76-00164: "Research and Development into New Technologies Associated with Low Cost Thin Film Solar Cells". (1977-78).

2.  J.I.B. Wilson and J. Woods; J. Phys. Chem. Solids 34, 171 (1973).

3.  G.A. Somorjai and N.R. Stemple; J. Appl. Phys. 35, 3398 (1964).

4.  J. Dresner and F.V. Shallcross; J. Appl. Phys. 34, 2390 (1963).

5.  L.L. Kazmerski et al; J. Appl. Phys. 43, 3521 (1972).

6.  P.H. Wendland; J. Opt. Soc. Am. 52, 581 (1962).

7.  G. Kuwabara; J. Phys. Soc. Jap. 9.1, 97 (1954).

8.  S.M. Sze "Physics of Semiconductor Devices" J. Wiley and Sons (1969).

9.  Jenkins and White "Fundamentals of Optics" McGraw Hill (1957).

10. T.M. Bieniewski and S.J. Czyzak; J. Opt. Soc. Am. 53, 496 (1963).

11. C.A. Escoffery; J. Appl. Phys., 35, 2273 (1964).

12. H. Okamoto; Jap. J. Appl. Phys. 4, 234 (1965).

13. H. Okamoto; Jap. J. Appl. Phys. 4, 821 (1965).

14. J. Dresner and F.V. Shallcross; Sol. St. Elect. 5, 205 (1962).

15. R.G. Mankarious; Sol. St. Elect. 7, 702 (1964).

16. F.I. Vergunas et al; Sov. Phys. Cryst. 11.3, 420 (1966).

17.    J. Shewchun et al; Rev. Sci. Instrum. $\underline{42}$, 1797 (1971).

18.    A.J. Behringer and L. Corrsin; J. Electrochem. Soc. $\underline{110\text{-}10}$, 1083 (1963).

19.    A. Waxman et al; J. Appl. Phys. $\underline{36.1}$, 168 (1965).

20.    H. Berger; Phys. Stat. Solidi. $\underline{1}$, 739 (1961).